# Pseudo-Single-Crystal Electrochemistry on Polycrystalline Electrodes: Visualizing Activity at Grains and Grain Boundaries on Platinum for the Fe^{2+}/Fe^{3+} Redox Reaction

Barak D. B. Aaronson,[†,‡] Chang-Hui Chen,[†,‡] Hongjiao Li,[§] Marc T. M. Koper,[§] Stanley C. S. Lai,[‡] and Patrick R. Unwin*,[‡]

[‡]Department of Chemistry, University of Warwick, Gibbet Hill Road, Coventry CV4 7AL, U.K.
[§]Leiden Institute of Chemistry, Leiden University, P.O. Box 9502, 2300 RA Leiden, The Netherlands

S *Supporting Information*
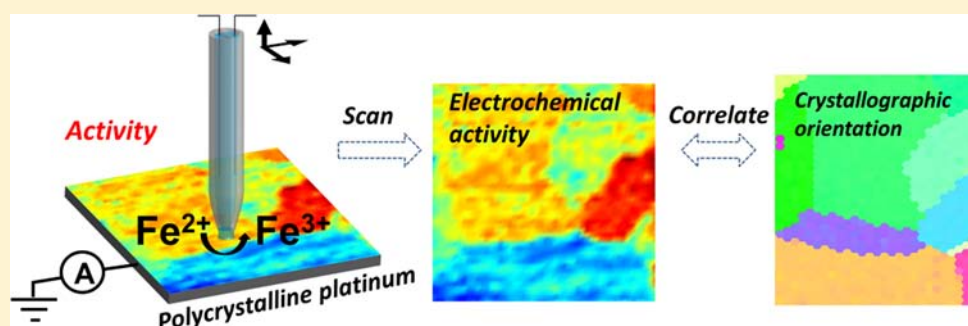
ABSTRACT: The influence of electrode surface structure on electrochemical reaction rates and mechanisms is a major theme in electrochemical research, especially as electrodes with inherent structural heterogeneities are used ubiquitously. Yet, probing local electrochemistry and surface structure at complex surfaces is challenging. In this paper, high spatial resolution scanning electrochemical cell microscopy (SECCM) complemented with electron backscatter diffraction (EBSD) is demonstrated as a means of performing 'pseudo-single-crystal' electrochemical measurements at individual grains of a polycrystalline platinum electrode, while also allowing grain boundaries to be probed. Using the $Fe^{2+/3+}$ couple as an illustrative case, a strong correlation is found between local surface structure and electrochemical activity. Variations in electrochemical activity for individual high index grains, visualized in a weakly adsorbing perchlorate medium, show that there is higher activity on grains with a significant (101) orientation contribution, compared to those with (001) and (111) contribution, consistent with findings on single-crystal electrodes. Interestingly, for Fe^{2+} oxidation in a sulfate medium a different pattern of activity emerges. Here, SECCM reveals only minor variations in activity between individual grains, again consistent with single-crystal studies, with a greatly enhanced activity at grain boundaries. This suggests that these sites may contribute significantly to the overall electrochemical behavior measured on the macroscale.

■ INTRODUCTION

Identifying correlations between the electrochemical activity and morphology (in particular, the crystallographic orientation) of electrode surfaces is of major fundamental importance toward achieving a better understanding of heterogeneous electron transfer (ET) processes. Moreover, the rational development of electrocatalysts,[1,2] for a variety of applications, from energy conversion and storage[3–7] to electrosynthesis[8,9] and electrochemical sensors,[10] requires knowledge of electrode structure–activity relationships. A major area of interest is the structure-dependent reactivity of platinum and other platinum-group metals, which have proven to be among the most efficient electrocatalysts for a wide variety of reactions.[11,12]

A common approach to investigating the relationship between surface structure and electrochemical activity is to employ well-defined single-crystal electrodes.[3,13,14] However, while valuable information can be obtained, such studies are challenging, as well as expensive and time-consuming, as each electrode needs to be carefully prepared, characterized, and handled so that only a single surface orientation is assured. Furthermore, the effect of boundaries between different crystallographic grains cannot be probed on such surfaces, even though they may play a significant (or possibly even dominant) role in surface reactivity.[15,16] These challenges could be circumvented if one could directly probe the local structure of a polycrystalline sample, for example with electron backscatter diffraction (EBSD),[17] and correlate this with localized electrochemical measurements.[17,18]

One approach for performing localized electrochemistry on a polycrystalline surface is to prepare an array of individually addressable micrometer scale electrodes through lithographic

processing.[17] However, due to the irregular shape and size of crystalline grains, the employment of lithographic techniques to expose specific grains is technically very demanding. Furthermore, lithographic processing is rather involved and can leave residual contaminations which may impact the reactivity of the electrode.[19,20] Another approach is to limit the contacted area of the working electrode by employing droplet based techniques.[18,21−23] However, methods of this type have tended to be restricted to static point-by-point measurements (usually on a large scale), and the mapping of an area of an electrode has proved to be time-consuming and difficult technically.

Recently, we introduced scanning electrochemical cell microscopy (SECCM)[21,24−29] as a new scanning probe technique to visualize ET processes quantitatively at the microscale and nanoscale. SECCM employs a dual barrel (theta) pipet (200 nm−2 μm diameter) probe that is scanned over an electrode surface of interest, while recording the current through the substrate as a function of xy-position. The effective potential of the substrate/solution interface is controlled via quasi-reference counter electrodes (QRCEs) in each channel of the theta pipet, and a potential difference between these electrodes also promotes an ion-conductance current which is used for feedback. The feedback is particularly stable when the probe is oscillated normal to the surface with a small amplitude, and the resulting alternating current (AC) component is measured at the oscillation frequency.[21,24−30] An attractive feature of SECCM is that each location on the electrode is only exposed to the electrolyte solution briefly, minimizing electrode fouling[21] and other undesired processes. In contrast to scanning electrochemical microscopy (SECM),[31,32] which is also powerful for visualizing heterogeneous electrode substrates,[33−36] SECCM measures the electrochemical processes of interest directly, in a manner that is similar to conventional dynamic electrochemistry, and readily achieves higher spatial resolution.

In this paper, we study the one-electron oxidation of Fe^{2+} to Fe^{3+} in aqueous media on a polycrystalline platinum surface with SECCM and correlate the local activity with the corresponding microscale crystallographic orientation of the surface determined by EBSD. The $Fe^{2+/3+}$ redox couple is especially interesting, as it is an ostensibly simple one-electron process, although showing strong kinetic limitations and often considered to be a model inner-sphere process based on macroscopic measurements on polycrystalline metal electrodes.[37] In our recent work on polycrystalline boron doped diamond, we have found electron transfer for this redox couple to be very strongly surface-sensitive.[21] Similar findings have been reported for other carbon electrode materials[38,39] as well as metal electrodes.[40] However, the origin of the structure-sensitivity is unclear and has been a topic of debate, with explanations ranging from differences in surface coordination of the $Fe^{2+/3+}$ species,[41] variations in the local density of electronic states of the electrode,[40] changes in double layer structure with the surface structure,[42−44] different crystallographic facets of an electrode having different potential of zero charge,[42,43] and/or effects due to surface sensitive anion adsorption.[45,46] Fe^{2+} oxidation on platinum is further complicated by the fact that it takes place at potentials at which oxidation of the platinum surface also occurs.[47] Platinum surface oxidation consists of a number of steps whose significance are time scale and potential dependent.[47,48] Initially, surface oxidation occurs through the fast, reversible formation of Pt−OH.[49] Further irreversible

oxidation to form PtO and PtO_2 occurs slowly over the course of seconds to tens of seconds. Thus, the electrochemical response for many redox reactions can be strongly impacted by the time scale of the measurement for potentials in the oxide formation region. This is particularly true for the $Fe^{2+/3+}$ redox process.[47,50] Based on our recent work,[21,24−29,33,51] SECCM provides a powerful method to investigate whether structural effects hold for the oxidation of Fe^{2+} on polycrystalline platinum.

We further demonstrate that SECCM coupled with EBSD is a powerful approach to perform 'pseudo-single-crystal' experiments on a polycrystalline (platinum) substrate. In particular, owing to the short contact time of SECCM, we show that we can obtain information on surface reactivity before (irreversible) surface oxidation sets in, allowing us to probe the structure−activity relationship for Fe^{2+} oxidation at significant overpotentials. Notably, we identify distinct patterns of spatial ET activity and anion effects, which provide a new view of heterogeneous redox reactions at polycrystalline platinum. This evidently has significant implications for kinetic and mechanistic studies at polycrystalline electrodes, generally, which are usually studied by macroscopic techniques, such as cyclic voltammetry, without the ability to assess whether reactions can be considered to be uniform across a substrate.

■ EXPERIMENTAL SECTION

All electrolyte solutions were prepared freshly from high purity water (Milli-Q, Millipore, 18.2 MΩ cm resistivity at 25 °C). $FeSO_4 \cdot 7H_2O$ ($\geq$99.0% purity, Sigma-Aldrich), $Fe(ClO_4)_2 \cdot xH_2O$ (98% purity, Sigma-Aldrich), H_2SO_4 (99.999% purity, Sigma-Aldrich), and $HClO_4$ ($\leq$0.001% chloride content, Acros) were used as received.

Single-crystal measurements were performed on bead-type single-crystal electrodes between 1 mm and 3 mm diameter, prepared according to Clavilier's method.[52] Prior to each experiment, the electrodes were flame annealed and allowed to cool down in a hydrogen/argon mixture (*ca.* 3:1) after which they were transferred to the electrochemical cell under the protection of a droplet of deoxygenated ultrapure water. A piece of platinum foil and a reversible hydrogen electrode (connected via a Luggin capillary) were employed as counter and reference electrode, respectively. All glassware was cleaned by boiling in a 1:1 mixture of nitric acid and sulfuric acid, followed by repeated boiling in ultrapure water.

In the SECCM imaging experiments, the substrate (working electrode) consisted of a polycrystalline platinum foil (>99.95%, 0.0125 mm thickness; Advent Research Materials), with a Pd−H_2 QRCE employed in each of the channels of the SECCM pipet. Before SECCM imaging, the Pt foil was cleaned by flame-annealing followed by potential cycling 200 times from 0 to 1.6 V and ending at 0 V to ensure an oxide-free surface.

The Pd−H_2 REs and QRCEs (E^0 = 50 mV vs the reversible hydrogen electrode)[53] were prepared by evolving hydrogen on a palladium wire (>99.95%, MaTeck) in a particular supporting electrolyte (either 10 mM H_2SO_4 or 10 mM $HClO_4$) until hydrogen bubbles were clearly visible on the surface of the wire, indicating hydrogen saturation. All potentials in this paper are reported relative to the Pd−H_2 RE or QRCE in the working solution.

The SECCM setup is shown schematically in Figure 1 and is discussed in detail in previous works.[24,29] Briefly, a tapered dual barrel (theta) pipet was pulled with a laser puller (P-2000; Sutter Instruments) to form a sharp tip with an outer diameter of ~1.5 μm. The size of the tip was measured accurately by scanning electron microscopy after the experiments by measuring the mirror tip, produced in the pulling process, which is closely identical. The exterior surface of the pulled pipet was rendered hydrophobic by immersing the tip in dichlorodimethylsilane (99+ % purity, Acros) while flowing argon gas through it at ~4 bar for one minute, followed by leaving the tip to dry in air, while argon was still flowed through for another two
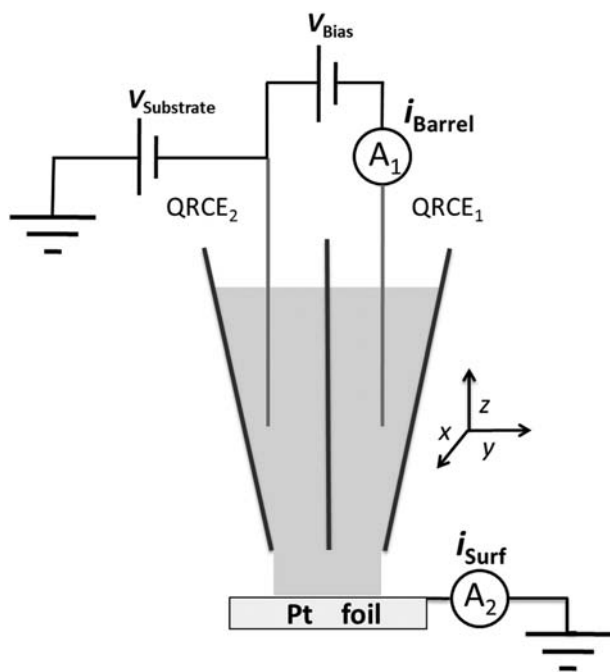
Figure 1. Schematic of scanning electrochemical cell microscopy (SECCM). A piece of platinum foil (see text) served as the working electrode. Pd−H$_2$ quasi-reference counter electrodes (QRCEs) were inserted into each barrel of a pipet, used as an imaging probe. $V_{Substrate}$: potential applied to the QRCE$_2$ (relative to ground); V_{bias}: potential bias applied between QRCE$_1$ and QRCE$_2$; i_{Barrel}: current between the QRCEs; i_{Surf}: current through the substrate.

minutes. Each barrel was filled with the solution of interest, and a Pd−H$_2$ QRCE was inserted into each barrel. A bias potential, V_{bias}, was applied between the QRCEs: 0.2 V for the HClO$_4$ study and 0.5 V for the H$_2$SO$_4$ study. During experiments, the z-piezoelectric positioner (perpendicular to the substrate) was oscillated at 70 Hz with 58 nm peak amplitude. This oscillation produced an alternating ion current between the barrels upon contact of the droplet at the end of the pipet with the working electrode substrate (platinum foil).[25] The resulting AC magnitude, typically in the range of 150 pA (∼ 2% of the mean conductance current), was used as a set point (feedback) to maintain a constant tip-to-substrate separation (meniscus height). The substrate electrode was connected to a high sensitivity current amplifier and held at ground. It typically experienced a potential that was the midpoint of the potential applied to the QRCEs but of opposite sign.[25]

SECCM images were constructed from parallel line scans with a spacing of 2 μm between each line. A data point (pixel) was recorded every 1.5 μm over a period of 40 ms at a frequency of 25 kHz (corresponding to the average of 1000 measurements). Prior to collecting data at each pixel, a 20 ms waiting time was applied to minimize currents due to double layer charging and the initial surface oxidation process (vide infra).

Electron backscatter diffraction (EBSD) images of platinum substrates were recorded on a Zeiss SUPRA 55 variable-pressure field emission scanning electron microscope (FE-SEM) at 20 kV on a 70° tilted sample with an EDAX TSL EBSD system. EBSD images were constructed from diffraction patterns recorded every 2 μm.

■ RESULTS AND DISCUSSION

Macroscopic Characteristics of the Fe^{2+}/Fe^{3+} Redox Couple on a Polycrystalline Platinum Foil. The one-electron oxidation of Fe^{2+} on a macroscopic scale was studied in both perchlorate and sulfate media on a polycrystalline platinum foil using cyclic voltammetry. Typical cyclic voltammograms (CVs) of 2 mM Fe^{2+} (from Fe(ClO$_4$)$_2$) in

10 mM HClO$_4$ and of 2 mM Fe^{2+} (from FeSO$_4$) in 10 mM H$_2$SO$_4$ (both ca. pH 2) are shown in Figure 2a. CVs in only the supporting electrolyte (without the Fe-salt) are shown in Figure 2b for comparison.
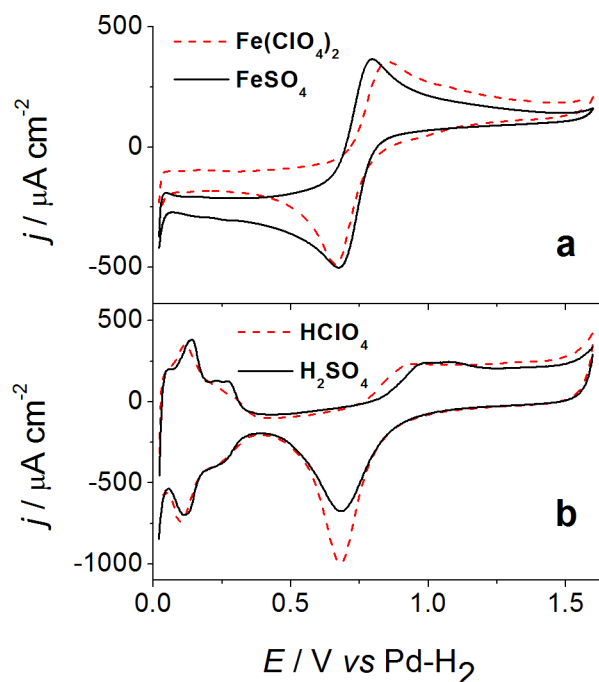

Figure 2. (a) Cyclic voltammograms of 2 mM Fe(ClO$_4$)$_2$ in 10 mM HClO$_4$ (red dashed line) and 2 mM FeSO$_4$ in 10 mM H$_2$SO$_4$ (black line); the scan rate was 25 mV s^{-1}. (b) Background voltammograms of 10 mM HClO$_4$ (red dashed line) and 10 mM H$_2$SO$_4$ (black line); the scan rate was 500 mV s^{-1}.

The onset potential for Fe^{2+} oxidation (Figure 2a) is nearly 100 mV lower in sulfate than in perchlorate, although beyond this the current density-potential waves are rather similar. The difference in onset potential between the two electrolytes is not due to any difference in the Fe$^{2+/3+}$ formal potential (E$^{0'}$): we have measured this to be the same in each medium (+0.85 V vs Pd−H$_2$). Rather, the CVs in electrolyte alone (Figure 2b) demonstrate significant differences in the surface oxidation state in each of the two media in the potential range close to E$^{0'}$ for Fe$^{2+/3+}$. The oxidation of platinum in the perchlorate medium starts about 100 mV more cathodic than in the sulfate medium. This can be attributed to the strong adsorption of the sulfate ions, inhibiting surface oxidation, compared to the weakly adsorbing perchlorate ions.[46,54] Generally, it can be seen that, in both sulfuric acid and perchloric acid, the oxidation of Fe^{2+} largely overlaps with the platinum surface oxidation region. These cyclic voltammograms were used to select potentials for SECCM imaging, ranging from the onset of oxidation toward the diffusion-limited region.

As highlighted above, one of the challenges in studying the one-electron Fe^{2+} oxidation on platinum is that the measured current could represent a contribution of both Fe^{2+} oxidation and surface oxide formation processes. Two measures were taken in order to distinguish between Fe^{2+} oxidation and surface oxidation processes in the SECCM setup: (i) allowing a short waiting time, to minimize the current due to double layer charging and Pt−OH formation; and (ii) limiting the time of the measurement at each data point, to reduce the influence of

slow surface oxidation processes (PtO and PtO_2 formation). To quantify the magnitude of the background current due to oxide formation processes on the same time scale as the SECCM measurements for Fe^{2+} oxidation, we recorded an electrochemical image of the platinum foil at a potential in only the oxide region in blank electrolyte (without Fe^{2+}) and found the current to be negligible (see Supporting Information, S1).

Fe^{2+} Oxidation on Platinum in Perchloric Acid Solution. In order to probe the inherent electrochemical activity of polycrystalline platinum toward the oxidation of Fe^{2+}, without the added complexity of a strongly adsorbing anion, we initially employed a perchloric acid solution as electrolyte. Multiple SECCM activity images for the oxidation of 2 mM $Fe(ClO_4)_2$ in 10 mM $HClO_4$ on the polycrystalline platinum were obtained in the same area of the substrate, while holding the working electrode surface at potentials ranging from 0.75 V (close to the onset potential) to 1.4 V (mass transport limited potential) based on the macroscopic CVs in Figure 2a.

Two representative SECCM activity images of one area of the platinum surface at 0.8 and 1.0 V are shown in Figure 3a and 3b, with the corresponding EBSD image of the same area in Figure 3c. Five regions, each with different activity, can be identified in the SECCM image and are labeled in Figure 3a (I–V). The relative activity of these regions (based on the surface current magnitude) is as follows: III > IV > V > II ≈ I. In addition, some variation in activity can be observed within the individual regions.

Comparing the EBSD and SECCM maps, it is evident that the regions of distinctly different electrochemical activity correspond to particular grain structure by EBSD (Table 1). Notably, grains which have substantial (101) character (grains III, IV, and V) generally appear more active than grains having more (001) and (111) character (grains I and II).

Upon closer inspection, there are variations in activity for the grains having mainly (101) character (III–V), with the most active grain (grain III) having some (111) character. This structure-dependent relative activity was evident at all investigated potentials and highlights that, on polycrystalline platinum, the Fe^{2+}/Fe^{3+} reaction rate is strongly structure-dependent at the microscopic level.

The impact of structure on electrochemical reaction rate is summarized quantitatively in Figure 4a, which shows the average surface current of the designated grain areas marked in Figure 3a, extracted from a series of SECCM activity maps, as a function of the electrode potential. From these current–potential (*I-E*) plots, it is evident that the surface current for all grains increases with the increasing potential (increasing driving force) as expected, based on macroscopic CV measurements on polycrystalline platinum (Figure 2a), but is evidently grain-dependent. Note, particularly, that the relative activities between different grains are consistent throughout the entire potential range. Grain III, which has (101) sites, exhibits the highest activity at all potentials, while grain II, which has (001) sites separated by short (111) terraces, exhibits the lowest activity at all potentials. Grains IV and V show intermediate activity between these two extremes, as highlighted above.

Reactivity trends deduced from SECCM on the microcrystalline grains might reflect the relative reactivity of single-crystal electrodes. In order to verify this, we recorded cyclic voltammograms for the oxidation of Fe^{2+} in perchlorate solution on low index platinum basal plane single-crystal electrodes. Typical voltammograms, for the three basal faces are shown in Figure 5. To limit damage to the single-crystal
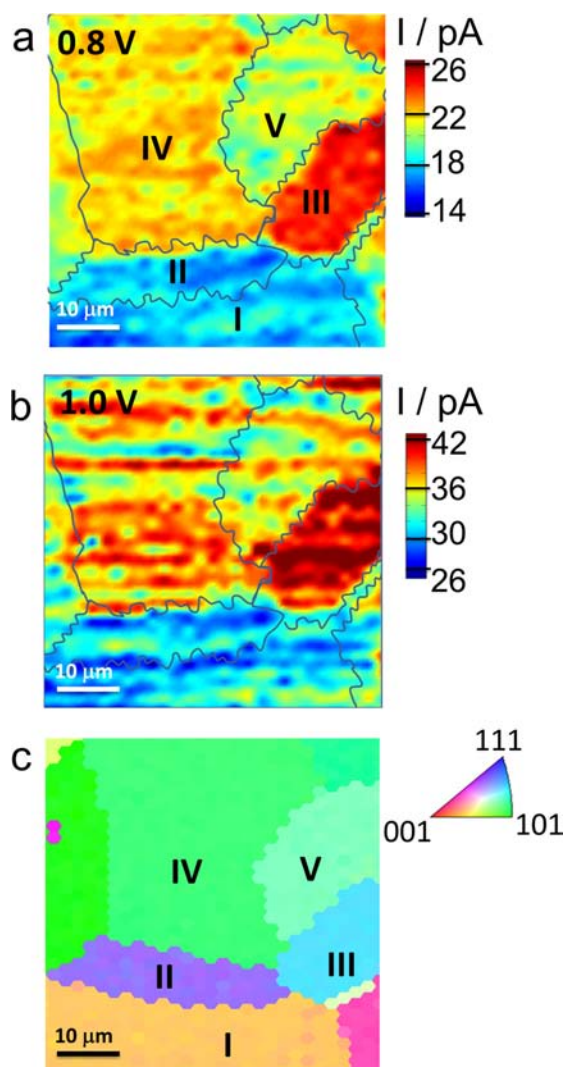

Figure 3. (a-b) Representative SECCM images of the oxidation of 2 mM Fe^{2+} to Fe^{3+} in 10 mM $HClO_4$ at 0.8 and 1.0 V relative to Pd–H_2. The five grains in the scanned regions are labeled "I", "II", "III", "IV", and "V". The boundaries between the grains deduced from EBSD are marked with blue lines to guide the eye. (c) Corresponding EBSD image (tilted roughly 10° in the *xy* plane compared to the SECCM images) with the color coded orientation map of the scanned area.

Table 1. Surface Orientations of Areas Marked in Figure 3

grain	approximate Miller index	description
I	(13 5 1)	mixed (001) and (101) character
II	(211)	(001) sites separated by short (111) terraces
III	(221)	(101) sites separated by short (111) terraces
IV	(771)	mainly (101) character
V	(651)	mainly (101) character

electrodes, due to irreversible oxide formation and reduction, the positive potential limit was restricted to 1.25 V. Within this potential window, Fe^{2+} oxidation on Pt(101) is clearly visible with an onset potential of *ca.* 0.7 V. On Pt(111) and Pt(001) the oxidation of Fe^{2+} starts at *ca.* 0.9 V, right below the anodic potential limit. Interestingly, this variation in onset potentials for Fe^{2+} oxidation closely mirrors the variations in the potentials of zero total charge (pztc) for the basal planes of platinum at pH 2, with a pztc of 0.18 V vs Pd–H_2 for Pt (101)
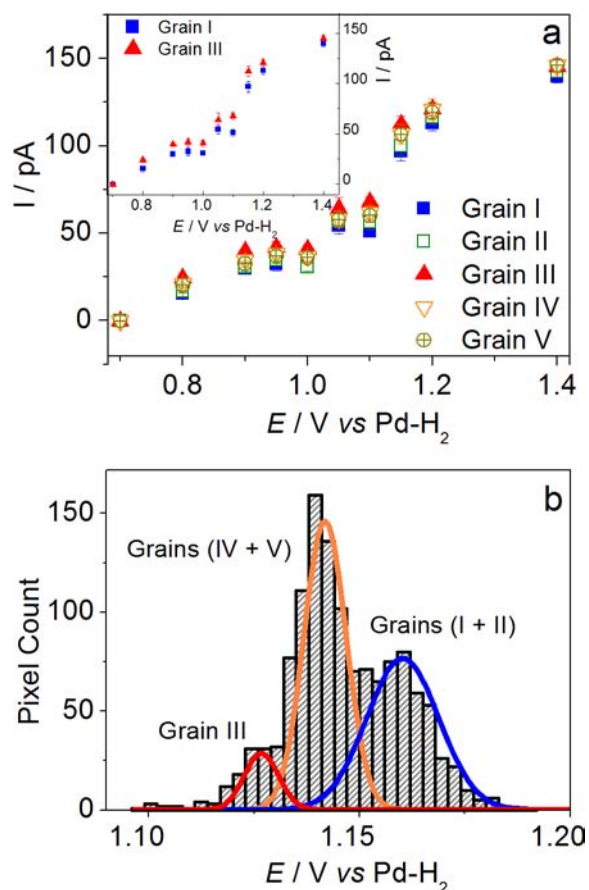
Figure 4. a) *I-E* curves of electrochemical current as a function of applied surface potential for 2 mM FeClO$_4$ in 10 mM HClO$_4$. The current is the average from regions of the SECCM images where grains were identified. Inset shows the *I-E* curves for grain "I" and grain "III" for clarity. b) Histogram of apparent half-wave potentials from spatially resolved *I-E* data at individual pixels in a series of SECCM images. Corresponding grains are labeled on the image.
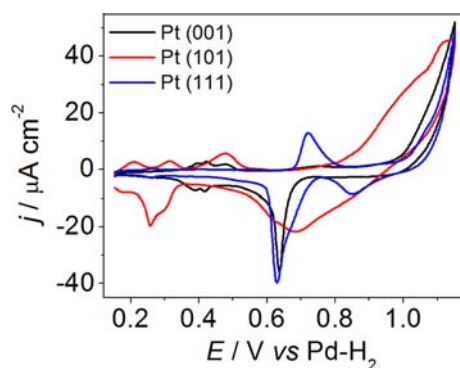

Figure 5. Cyclic voltammograms of 2 mM Fe(ClO$_4$)$_2$ in 10 mM HClO$_4$ on Pt(111) electrode (blue line), Pt(001) electrode (black line), and Pt(101) electrode (red line). Scan rate was 10 mV s^{-1}.

and 0.39 and 0.38 V for Pt (111) and Pt (001), respectively.[55] This correspondence may suggest that the structure-sensitive activity for the oxidation of Fe^{2+} originates from variations of pztc, which strongly affects the double layer.[42,43]

Thus, it is evident that the single-crystal findings are qualitatively consistent with the trend in reactivity obtained from SECCM, confirming the validity of the SECCM approach. However, it is important to note that the variation between the

electrochemical activities of single-crystal basal planes is much more pronounced than the variations between the different grains on the polycrystalline substrate. This is because grains on the polycrystalline substrate do not possess true basal-plane orientation but are high index facets with contributions of all three basal planes. Some variation in orientation within a single grain (seen as slight color variations in Figure 3c) may also be attributed to the variation of surface current within the individual grains (Figure 3a-b). On the other hand, a very positive outcome of the EBSD study, coupled with SECCM, is that high index facets can readily be investigated; such facets are extremely difficult to prepare and maintain as macroscopic single crystals.

The variations in reactivity in the SECCM images can further be analyzed quantitatively on a point-by-point basis. For each of the 1271 measurement points in an image, individual *I-E* curves were constructed (i.e., 1271 *I-E* curves, each with 10 points), and the half-wave potential corresponding to 75 pA (half the mass transport limited current) for each *I-E* curve was extracted. The distribution of these apparent half-wave potentials is shown in Figure 4b and can be deconvoluted into three prominent individual Gaussian distributions, centered around 1.16, 1.14, and 1.13 V. Based on the number of counts in each distribution, as well as the relative activity of the grains, we can assign the distribution centered around 1.16 V to grains I and II, the distribution around 1.14 V to grains IV and V, and the distribution around 1.13 V to grain III. It is worthwhile noting that the variation in apparent half-wave potentials spans for 0.03 V, which might be considered relatively small, but is readily detected in the SECCM experiments. The peaks in the observed half-wave potential distributions for the individual grains correspond to estimated electron transfer rate constants (k^0) of 1.1×10^{-4} cm s^{-1}, 1.9×10^{-4} cm s^{-1}, and 1.6×10^{-4} cm s^{-1} for grains I + II, III, and IV + V, respectively (see Supporting Information, S2). These values fall within the wide range of k^0 values previously reported for the Fe$^{2+/3+}$ couple on platinum in perchloric acid electrolyte, which vary from $\sim 10^{-5}$ cm s^{-1} to $\sim 10^{-3}$ cm s^{-1}.[58,59] This wide range has been ascribed to the strong sensitivity of the Fe$^{2+/3+}$ couple toward the state of the electrode surface, which can be impacted by variations in surface roughness and the presence of trace contaminants (such as strongly adsorbing anions).[58,60]

It is important to point out that the local variation in activity visualized by SECCM would have some impact on macroscopic CV measurements of heterogeneous ET on polycrystalline platinum. Electrode kinetic measurements on polycrystalline platinum tend to implicitly assume a uniform electrode surface,[45,46,56,57] and evidently, at least for the case of Fe^{2+}/Fe^{3+} (and perhaps other reactions), this is not always appropriate.

Finally, to exclude the possibility that the observed variations in surface current between grains are due to variations in roughness of the surface at individual grains, atomic force microscopy (AFM) images of the Pt foil were recorded and analyzed, showing average roughness (R$_a$) of 5.46 ± 0.5 nm (1 σ) with little variation between individual grains (see Supporting Information, S3). In order to further investigate the possibility of droplet size variance during the SECCM scan, a control image was recorded on the polycrystalline Pt foil for the outersphere redox mediator ferrocenylmethyltrimethylammonium (FcTMA$^+$), at the half-wave potential, and little variation in the surface current across the sample, that could be

related to variations in wetting, was seen (see Supporting Information, S4).

Fe^{2+} Oxidation in Sulfate Medium. To investigate the possible role of anion adsorption, we examined Fe^{2+} oxidation on polycrystalline platinum in sulfuric acid, in which sulfate anions absorb specifically.[61] It has been suggested previously that sulfate, or other specifically adsorbed anions (such as Cl^- and Br^-), can facilitate Fe^{2+} oxidation by acting as a bridge for electron transfer or by modifying the electrical double layer.[62] Given that sulfate adsorption on platinum surfaces is facet sensitive,[63,64] one might expect that the activity for Fe^{2+} oxidation could be affected accordingly.

Eight SECCM electrochemical activity maps for the oxidation of 1 mM Fe^{2+} in 10 mM H_2SO_4 were obtained by holding the surface at potentials ranging from 0.75 to 1.3 V, based on macroscopic CVs (Figure 2a). Figures 6a and 6b show two representative SECCM activity maps at 0.8 and 1.0 V. The corresponding EBSD map for the area imaged with SECCM is sh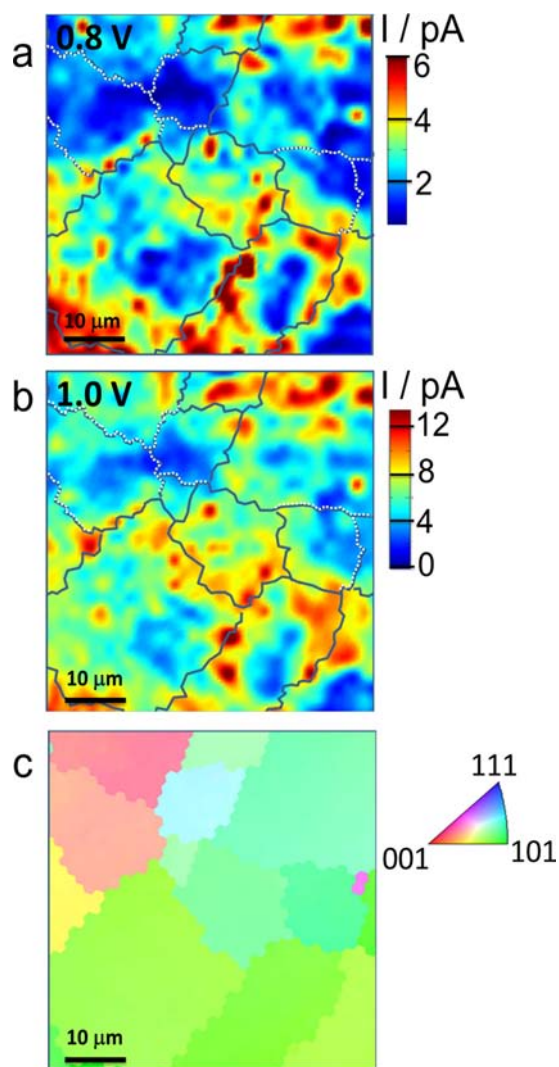own in Figure 6c. From the EBSD map, it can be seen that most of the grains within the area investigated have a significant contribution of (101) orientation with a fraction of grains with a main contribution from (001) orientation. Although the imaged area does not include all basal planes, some striking features are exhibited. By comparing the EBSD and SECCM maps, it is clearly evident that a correlation exists between structure and activity in sulfuric acid, but it is that the activity of the surface is strongly dominated by grain boundaries, with the grains themselves also having some lower activity. This pattern of activity is in stark contrast with the results in the nonadsorbing perchlorate medium where no enhanced activity was detectable at the boundaries between the crystalline grains.

Closer inspection of the maps in Figure 6 further highlights that while some grain boundaries exhibit a strongly enhanced activity, this is not generally true of all grain boundaries. Indeed, grain boundaries deduced from the EBSD map, and marked with white dotted lines on the SECCM maps, do not display enhanced activity in any of the eight images at the wide range of potentials covered. These electrochemically 'invisible' boundaries encompass grains closer to the (001) orientation, while the more active grain boundaries are those that encompass grains close to the (101) orientation, indicating that there may be an effect of the character of the grain boundary itself.

Cyclic voltammograms of the $Fe^{2+/3+}$ redox reaction in sulfate medium on basal plane single-crystal electrodes (Figure 7) show minimal differences in activity between basal planes in
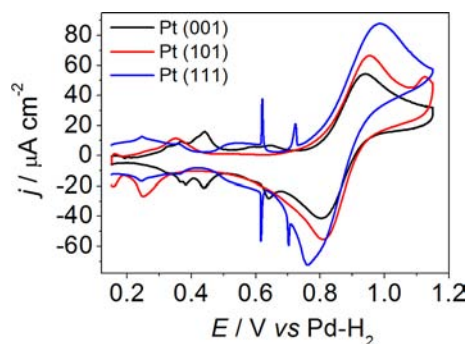

Figure 6. (a-b) SECCM images of the oxidation of 1 mM Fe^{2+} to Fe^{3+} in 10 mM H_2SO_4 at 0.8 and 1.0 V relative to Pd−H_2. Grain boundaries (from EBSD) are marked with either black lines (boundaries at which an enhanced current was observed) or white dotted lines (with no enhanced current) to guide the eye. (c) Corresponding EBSD image and surface orientation of the same area.

Figure 7. Cyclic voltammograms of 2 mM $FeSO_4$ in 10 mM H_2SO_4 on Pt(111) electrode (blue line), Pt(001) electrode (black line), and Pt(101) electrode (red line) vs Pd−H_2. Scan rate was 10 mV s^{-1}.

the potential region for the oxidation of Fe^{2+}, which is in agreement with our SECCM findings for the areas within the grains, which show more or less similar activities. The differences in peak currents for the single-crystal measurements may be attributed to the variations in oxide formation on different facets which inhibit the oxidation of Fe^{2+}.[47] The important point here, however, is that single-crystal measurements cannot reveal any electrochemical information on the grain boundaries, emphasizing a key advantage of SECCM for probing the electrochemical response of complex materials at high resolution, in this case the boundaries between crystalline grains.

The differences between the activity of grains and grain boundaries can be seen in the I-E plots in Figure 8, constructed for these different areas from analysis of images at various potentials, from the onset potential to approaching the mass transport limited potential. As in the case of perchlorate, the trend of surface current increase with the increase of the potential (driving force) is clearly seen for both grain boundary areas and areas within grains, but grain boundary areas show
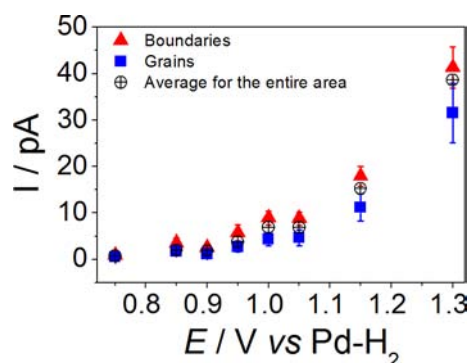
Figure 8. *I-E* curves for 1 mM FeSO$_4$ in 10 mM H$_2$SO$_4$. The current was obtained by averaging the current from regions of the SECCM images where grain boundaries (▲, red) and regions within the boundaries (■, blue) were identified. Similarly, an *I-E* curve for the average current over the entire scanned region (including all grains and boundaries) is also shown (⊕) for comparison.

higher activity at all potentials. These findings highlight clearly that certain grain boundaries exhibit a strongly enhanced activity toward Fe^{2+} oxidation. A further understanding of the structure of these boundaries and their role in surface reactivity would be beneficial, not only for Fe^{2+} oxidation but also for other surface dependent reactions as well.

Although uncertainty in the size of the grain boundary prevents a full kinetic analysis, an estimate of the grain boundary activity can be made. Between 0.8 and 1.15 V, the SECCM current at active boundaries is about twice than that in the neighboring grains. Analysis of the AFM images of a polycrystalline Pt foil yielded an estimated upper limit of grain boundary width of ~50 nm (Supporting Information, S3), which accounts for about 4% of the area encompassed under the 1.5 μm diameter SECCM pipet. This suggests that the grain boundaries are at least 30-fold more active than the areas within the grain.

An important feature of SECCM is that the facilitated migration current across the meniscus at the end of the tip, between the two QRCEs, also enhances mass transport of charged species to and from the substrate of investigation. The mass transport coefficient for an electrode in SECCM is estimated[25] to be about 10−20 times higher than in macroscale measurements and this leads to a much more drawn out current−voltage response in SECCM (Figure 8). The same effect on the shape of the wave can be seen for the perchlorate medium when inspecting the macroscale CV. However, the SECCM assisted mass transport rate depends on the charge of the species in solution and on the magnitude of the migration current. Thus, when examining the SECCM results for perchlorate and sulfate media side by side, differences in mass transport of the systems and Fe^{2+} concentration (1 mM and 2 mM for the sulfate and perchlorate, respectively) need to be taken into consideration. The transport limited current in perchlorate (Figure 4a at 1.4 V) is about four times higher than that observed in sulfate medium (Figure 8 at 1.3 V). This is due to the different concentrations used and differences in mass transport coefficients for the two electrolytes, which depends on speciation (e.g., ion pairing) and the potential bias between the QRCEs. In the sulfate medium, the dominant species is FeHSO$_4^+$ (with some Fe^{2+} and FeSO$_4$), whereas in the perchlorate medium Fe^{2+} and Fe^{3+} remain largely free.[65,66] Regardless, the main point is the significantly different patterns

of local activity for the Fe$^{2+/3+}$ couple in the two media at polycrystalline platinum, which are readily revealed for the first time by SECCM.

CONCLUSIONS

Conventional macroscopic electrochemical measurements at polycrystalline metal electrodes, such as platinum, have tended to implicitly assume a uniformly active surface. The studies presented herein show that this is not a reasonable assumption for polycrystalline platinum, at least for the model Fe$^{2+/3+}$ system. Indeed, considering heterogeneous electron transfer (ET) rates to be uniform across a polycrystalline surface may not only lead to misinterpretation of kinetic data but also ignores subtle electrode structure effects which are essential to gaining a deeper understanding of fundamental electrochemical processes. Such effects are readily revealed by SECCM, which provides a powerful approach for visualizing electrode activity.

By comparing the activity of individual grains, deduced by SECCM, to grain structure from EBSD images, we have found that the electrochemical oxidation of Fe^{2+} is sensitive to the platinum surface orientation, regardless of the supporting electrolyte. Moreover, we have established that grain boundaries can play an important role in this rather complex electrochemical process.

The main features of the SECCM technique in the present application are that (i) it allows 'pseudo-single-crystal' experiments (in individual grains of a polycrystalline sample with high index facets and grain boundaries) owing to the spatial confinement of the electrochemical cell; (ii) it allows access to fast surface kinetic effects owing to the higher mass transport rates generated; and (iii) it enhances the resolution with respect to competing processes (such as surface oxidation) with the ability to fine-tune the time regime in which measurements are made. Thus, Fe^{2+} oxidation in perchlorate medium was found to exhibit variations in rate (current) depending on the crystallographic orientation of the microcrystalline grain, with a trend that could be rationalized to a large extent based on cyclic voltammograms obtained on basal plane (low index) single-crystal electrodes. In contrast, in sulfate medium, boundaries between grains exhibited significantly higher reactivity (at least an order of magnitude) compared to the areas within grains.

The studies herein provide a platform for further investigation of polycrystalline electrode materials, particularly for those of electrocatalytic relevance. More generally, the data presented have major implications for the investigation and analysis of electrochemical processes by macroscopic techniques, which evidently average the reactivity over many different types of surface sites. SECCM provides a means of probing individual sites effectively and unambiguously.

ASSOCIATED CONTENT

Ⓢ Supporting Information

SECCM background image in supporting electrolyte, k^0 calulations, AFM image of platinum and SECCM image for FcTMA$^+$ oxidation. This material is available free of charge via the Internet at http://pubs.acs.org.

AUTHOR INFORMATION

Corresponding Author
E-mail: P.R.Unwin@warwick.ac.uk.
Author Contributions
[†]These authors have contributed equally.

REFERENCES

(1) Bard, A. J. *J. Am. Chem. Soc.* **2010**, *132*, 7559.

(2) Somorjai, G. A. *Science* **1985**, *227*, 902.

(3) Marković, N. M.; Ross, P. N., Jr. *Surf. Sci. Rep.* **2002**, *45*, 117.

(4) *Fuel Cell Catalysis: A Surface Science Approach*; Wiley: Hoboken, NJ, 2009.

(5) Kato, H.; Asakura, K.; Kudo, A. *J. Am. Chem. Soc.* **2003**, *125*, 3082.

(6) Arico, A. S.; Bruce, P.; Scrosati, B.; Tarascon, J.-M.; van Schalkwijk, W. *Nat. Mater.* **2005**, *4*, 366.

(7) Lee, S. W.; Chen, S.; Suntivich, J.; Sasaki, K.; Adzic, R. R.; Shao-Horn, Y. *J. Phys. Chem. Lett.* **2010**, *1*, 1316.

(8) Couper, A. M.; Pletcher, D.; Walsh, F. C. *Chem. Rev.* **1990**, *90*, 837.

(9) Lee, I.; Morales, R.; Albiter, M. A.; Zaera, F. *Proc. Natl. Acad. Sci. U. S. A.* **2008**, *105*, 15241.

(10) Sherigara, B. S.; Kutner, W.; D'Souza, F. *Electroanalysis* **2003**, *15*, 753.

(11) Rabis, A.; Rodriguez, P.; Schmidt, T. J. *ACS Catal.* **2012**, *2*, 864.

(12) Antolini, E. *Energy Environ. Sci.* **2009**, *2*, 915.

(13) Climent, V.; Feliu, J. M. *J. Solid State Electrochem.* **2011**, *15*, 1297.

(14) Koper, M. T. M. *Nanoscale* **2011**, *3*, 2054.

(15) Cherstiouk, O. V.; Gavrilov, A. N.; Plyasova, L. M.; Molina, I. Y.; Tsirlina, G. A.; Savinova, E. R. *J. Solid State Electrochem.* **2008**, *12*, 497.

(16) Maillard, F.; Savinova, E. R.; Stimming, U. *J. Electroanal. Chem.* **2007**, *599*, 221.

(17) König, U.; Davepon, B. *Electrochim. Acta* **2001**, *47*, 149.

(18) Schultze, J. W.; Pilaski, M.; Lohrengel, M. M.; Konig, U. *Faraday Discuss.* **2002**, *121*, 211.

(19) Dudin, P. V.; Snowden, M. E.; Macpherson, J. V.; Unwin, P. R. *ACS Nano* **2011**, *5*, 10017.

(20) Heller, I.; Kong, J.; Heering, H. A.; Williams, K. A.; Lemay, S. G.; Dekker, C. *Nano Lett.* **2004**, *5*, 137.

(21) Patten, H. V.; Lai, S. C. S.; Macpherson, J. V.; Unwin, P. R. *Anal. Chem.* **2012**, *84*, 5427.

(22) Day, T. M.; Unwin, P. R.; Macpherson, J. V. *Nano Lett.* **2006**, *7*, 51.

(23) Williams, C. G.; Edwards, M. A.; Colley, A. L.; Macpherson, J. V.; Unwin, P. R. *Anal. Chem.* **2009**, *81*, 2486.

(24) Ebejer, N.; Schnippering, M.; Colburn, A. W.; Edwards, M. A.; Unwin, P. R. *Anal. Chem.* **2010**, *82*, 9141.

(25) Snowden, M. E.; Güell, A. G.; Lai, S. C. S.; McKelvey, K.; Ebejer, N.; O'Connell, M. A.; Colburn, A. W.; Unwin, P. R. *Anal. Chem.* **2012**, *84*, 2483.

(26) Lai, S. C. S.; Patel, A. N.; McKelvey, K.; Unwin, P. R. *Angew. Chem., Int. Ed.* **2012**, *51*, 5405.

(27) Miller, T. S.; Ebejer, N.; Güell, A. G.; Macpherson, J. V.; Unwin, P. R. *Chem. Commun.* **2012**, *48*, 7435.

(28) Güell, A. G.; Ebejer, N.; Snowden, M. E.; McKelvey, K.; Macpherson, J. V.; Unwin, P. R. *Proc. Natl. Acad. Sci. U. S. A.* **2012**, *109*, 11487.

(29) Lai, S. C. S.; Dudin, P. V.; Macpherson, J. V.; Unwin, P. R. *J. Am. Chem. Soc.* **2011**, *133*, 10744.

(30) Rodolfa, K. T.; Bruckbauer, A.; Zhou, D.; Korchev, Y. E.; Klenerman, D. *Angew. Chem., Int. Ed.* **2005**, *44*, 6854.

(31) Mirkin, M. V.; Nogala, W.; Velmurugan, J.; Wang, Y. *Phys. Chem. Chem. Phys.* **2011**, *13*, 21196.

(32) Wittstock, G.; Burchardt, M.; Pust, S. E.; Shen, Y.; Zhao, C. *Angew. Chem., Int. Ed.* **2007**, *46*, 1584.

(33) Patten, H. V.; Meadows, K. E.; Hutton, L. A.; Iacobini, J. G.; Battistel, D.; McKelvey, K.; Colburn, A. W.; Newton, M. E.; Macpherson, J. V.; Unwin, P. R. *Angew. Chem., Int. Ed.* **2012**, *51*, 7002.

(34) Amemiya, S.; Bard, A. J.; Fan, F.-R. F.; Mirkin, M. V.; Unwin, P. R. *Annu. Rev. Anal. Chem.* **2008**, *1*, 95.

(35) Basame, S. B.; White, H. S. *J. Phys. Chem.* **1995**, *99*, 16430.

(36) Bath, B. D.; Lee, R. D.; White, H. S.; Scott, E. R. *Anal. Chem.* **1998**, *70*, 1047.

(37) Albery, J. *Electrode Kinetics*; Oxford University Press; 1975.

(38) McCreery, R. L. *Chem. Rev.* **2008**, *108*, 2646.

(39) Chen, P.; Fryling, M. A.; McCreery, R. L. *Anal. Chem.* **1995**, *67*, 3115.

(40) Samec, Z. *J. Electrochem. Soc.* **1999**, *146*, 3349.

(41) Nagy, Z.; Curtiss, L. A.; Hung, N. C.; Zurawski, D. J.; Yonco, R. M. *J. Electroanal. Chem.* **1992**, *325*, 313.

(42) Fawcett, W. R. *Electrochim. Acta* **1997**, *42*, 833.

(43) Fawcett, W. R.; Fedurco, M.; Kováčová, Z. *J. Electrochem. Soc.* **1994**, *141*, L30.

(44) Hromadova, M.; Fawcett, W. R. *J. Phys. Chem. A* **2001**, *105*, 104.

(45) Bochmann, H. G.; Vielstich, W. *Electrochim. Acta* **1988**, *33*, 805.

(46) Rodriguez-Lopez, J.; Bard, A. J. *J. Am. Chem. Soc.* **2010**, *132*, 5121.

(47) Rodríguez-López, J.; Minguzzi, A.; Bard, A. J. *J. Phys. Chem. C* **2010**, *114*, 18645.

(48) Angerstein-Kozlowska, H.; Conway, B. E.; Sharp, W. B. A. *J. Electroanal. Chem.* **1973**, *43*, 9.

(49) Schouten, K. J. P.; van der Niet, M. J. T. C.; Koper, M. T. M. *Phys. Chem. Chem. Phys.* **2010**, *12*, 15217.

(50) Imai, H.; Izumi, K.; Matsumoto, M.; Kubo, Y.; Kato, K.; Imai, Y. *J. Am. Chem. Soc.* **2009**, *131*, 6293.

(51) Güell, A. G.; Ebejer, N.; Snowden, M. E.; Macpherson, J. V.; Unwin, P. R. *J. Am. Chem. Soc.* **2012**, *134*, 7258.

(52) Clavilier, J.; Armand, D.; Sun, S. G.; Petit, M. *J. Electroanal. Chem. Interfacial Electrochem.* **1986**, *205*, 267.

(53) Vasile, M. J.; Enke, C. G. *J. Electrochem. Soc.* **1965**, *112*, 865.

(54) Inzelt, G.; Berkes, B. B.; Kriston, Á. *Pure Appl. Chem.* **2011**, *83*, 269.

(55) Garcia-Araez, N.; Climent, V.; Feliu, J. *J. Phys. Chem. C* **2009**, *113*, 9290.

(56) Bockris, J. O. M.; Mannan, R. J.; Damjanovic, A. *J. Chem. Phys.* **1968**, *48*, 1898.

(57) Łosiewicz, B.; Jurczakowski, R.; Lasia, A. *Electrochim. Acta* **2012**, *80*, 292.

(58) Weber, J.; Samec, Z.; Marecek, V. *J. Electroanal. Chem.* **1978**, *89*, 271.

(59) Angell, D. H.; Dickinso., T. *J. Electroanal. Chem.* **1972**, *35*, 55.

(60) Galizzio, D.; Trasatti, S. *J. Electroanal. Chem.* **1973**, *44*, 367.

(61) Kunimatsu, K.; Samant, M. G.; Seki, H. *J. Electroanal. Chem.* **1989**, *258*, 163.

(62) Johnson, D. C.; Resnick, E. W. *Anal. Chem.* **1977**, *49*, 1918.

(63) Nart, F. C.; Iwasita, T.; Weber, M. *Electrochim. Acta* **1994**, *39*, 2093.

(64) Mostany, J.; Herrero, E.; Feliu, J. M.; Lipkowski, J. *J. Phys. Chem. B* **2002**, *106*, 12787.

(65) Gil, A. F.; Salgado, L.; Galicia, L.; González, I. *Talanta* **1995**, *42*, 407.

(66) Sutton, J. *Nature* **1952**, *169*, 71.